Local Heat Transfer Characteristics of Multi Jet Impingement on High Temperature Plate Surfaces

Article *in* ISIJ International · January 2018

DOI: 10.2355/isijinternational.ISIJINT-2017-154

6 authors, including:

Wang Bingxing
Northeastern University (Shenyang, China)
38 PUBLICATIONS **308** CITATIONS

SEE PROFILE

ISIJ International, Vol. 58 (2018), No. 1, pp. 132–139

Local Heat Transfer Characteristics of Multi Jet Impingement on High Temperature Plate Surfaces

Bingxing WANG,* Dong LIN, Bo ZHANG, Lei XIONG, Zhaodong WANG and Guodong WANG

The State Key Laboratory of Rolling and Automation (RAL), Northeastern University, Shenyang, 110819 China.

(*Received on April 6, 2017; accepted on September 26, 2017*)

In order for the hot plate TMCP ultra-fast cooling technology to be optimized, the local heat transfer characteristics of multi jet impinging on hot plate surfaces were investigated. The experiments were performed for double and three jet impingement cooling study as cooling header primary units in the industrial scale. The jet velocity at the nozzle exit ranged between 1.99 m/s and 6.63 m/s. The results demonstrated that both the hydrodynamic structure and the heat transfer region distribution of multi jet impingement cooling were distinct from the single jet case. The parallel flows with a sufficient kinetic energy collided and intensified the heat transfer efficiency in the interference region. The higher-sized nozzle spacing magnified the heat exchange differences in the interference region, whereas the jet velocity increased both the heat flux and the rewetting velocity acceleration outside the stagnation region. The surface temperature in the interference region dropped slightly faster than the parallel flow region at the same spatial distance from the stagnant point, second only to the stagnant point, which was interpreted that the parallel flows interaction and agitation enhanced the heat transfer intensity. The results were valuable in the nozzle arrays arrangement and the heat transfer ability and cooling uniformity improvement of the ultra-fast cooling technology in industrial applications.

KEY WORDS: ultra-fast cooling; multi jet impingement; heat transfer region; heat flux; heat transfer coefficient.

1. Introduction

The Thermo-Mechanical Control Process (TMCP) is one of the most crucial technologies for steel production due to the corresponding significance in the microstructural and mechanical properties improvement of hot rolled steels. Recently, the ultra-fast cooling (UFC)[1–3] was developed in the controlled cooling by the water jet impingement technology with a heat flux reaching up to 10 MW/m^2.[4] Also, the typical concentrated header, consisting of hundreds of round nozzles is illustrated in **Fig. 1**. Apparently, both the heat transfer ability and the cooling uniformity of the cooling system were affected by the heat transfer characteristics of jet impingement depending on the jet velocity, nozzle diameter and nozzle arrangement.

Over the past few decades, numerous efforts were devoted to the factors investigations that affect the heat transfer characteristics. In addition, most researchers focused on the single jet impingement cooling. Robidou *et al.*[5] and Karwa *et al.*[6] studied the boiling heat transfer phenomenon and identified the boiling regimes by the snapshots observations and the boiling curves analysis. A high number of researchers investigated the rewetting phenomenon during water jet impingement,[7,8] characterizing the critical transfer from the film boiling regime to the nucleate boiling regime. It was concluded that the rewetting during the transient cooling could be regulated by affecting parameters, such as the rewetting temperature and the rewetting delay time. Other scientists confirmed that the superheat, the subcooling, the impingement direction and angle, the jet velocity and the coolant property strongly affect the heat transfer more or less.[9–12] The latter research works contributed in the basic heat transfer characteristics observation of the single jet impingement cooling.

Moreover, certain researchers performed the impingement cooling technology on the multi jet heat transfer mechanism. Kwon *et al.*[13,14] numerically studied the cooling of a steel plate in a run out table (ROT). The residual water thickness increased along with the flow rate. The cooling efficiency decreased along with the nozzle arrangement density, whereas the average heat flux did not increase monotonously along with the flow rate increase. Xie *et al.*[15] studied the both the surface flow field and the heat transfer of a high temperature plate cooled by nine-nozzle arrays with various Reynolds numbers. The results demonstrated that the maximum heat flux, the corresponding surface temperature and time period at each measurement point were dependent on the distance from both the impinging point and the jet velocity. Nallathambi *et al.*[16] estimated the heat flux in the metal quenching by an array of jets and reported that the wetting front, which separated the film boiling and nucleate boiling zones, changed the heat flux order. The maximum heat flux position and the corresponding propagation veloc-

* Corresponding author: E-mail: wbxang@126.com
DOI: http://dx.doi.org/10.2355/isijinternational.ISIJINT-2017-154

ity were plotted as a function of time. Fu *et al.*[17] focused on the water temperature and roll speed effects on the cooling rate in the thickness direction of an ultra-heavy plate under the multi jet impingement cooling.

In contrast, a high number of researchers usually studied the air jet impinging in the microelectronic technique field, such as the CPU cooling. LEON F. G. GEERS[18] focused on both pressure and velocity distribution characteristics, which were similar to the water cooling condition. Kercher and Tabakoff[19] presented the spatially-averaged surface heat transfer coefficients beneath an array of impinging jets with an in-line arrangement, whereas the results demonstrated that the Reynolds number and the streamwise/spanwise hole spacing were the most important parameters which affected all magnitudes of the spatial-averaged heat transfer coefficients. Metzger *et al.*[20] indicated that the in-line jet arrangement hole pattern could provide an improved heat transfer than the staggered arrangements for the Reynolds numbers from 5×10^3 to 2×10^4. The information from the aforementioned literature provided a profound insight into the multi jet impingement. Besides, most researches focused on the overall heat transfer characteristics of the cooling boundary, indifferently to the local heat transfer characteristics among the multi impinging jets, which severely determined both the cooling capacity and the local cooling uniformity.

In the present study, the experiments were performed for the local heat transfer behavior study of the multi jet. The effects of both nozzle spacing and jet velocity on the heat transfer capacity and the cooling uniformity were systematically studied for industrial applications. Special emphasis was laid on the heat transfer region distribution, the heat flux and the heat transfer coefficient (HTC). The research work herein would contribute to the nozzle arrangement optimization and the heat transfer ability and cooling uniformity improvement of the ultra-fast cooling technology in industrial applications.

2. Experimental Procedure

2.1. Experimental Model

The typical in-line and staggered jet arrangement patterns of high density cooling header for the industrial scale pilot ultra-fast cooling facility are presented in **Fig. 2**. Apparently, the double jet and the three jet were the primary units of either in-line or staggered jet arrangements. Also, the heat transfer behavior was affected dramatically by the nozzle diameter, nozzle spacing, jet velocity and the nozzle arrangement.

2.2. Experimental Setup and Procedure

The repeatable experimental plan is presented in **Fig. 3**. The AISI 304 L steel plate with the dimensions of 20 mm × 80 mm × 150 mm was utilized, due to the corresponding stability properties.[21] 15 holes were utilized in the thermocouples fixing, having been drilled to the depth of 30 mm. Also, the 3-mm Type K Chromel-alumel thermocouples were embedded for the temperature to be accessed at the position of −2.5 mm beneath the plate surface. 9 thermocouples were placed in the longitudinal direction according to the experimental requirements and another thermocouple

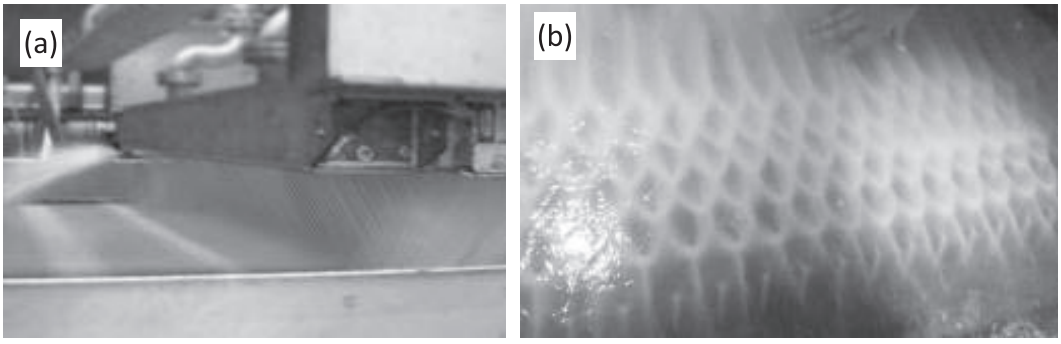

Fig. 1. Image of the high density cooling header during ultra-fast cooling process for hot rolling.

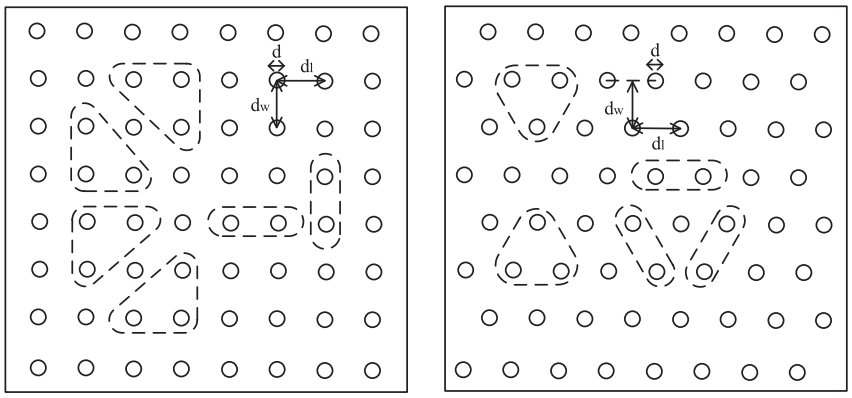

(a)In-line jet arrangement (b) Staggered jet arrangement

Fig. 2. Nozzles arrangement for the high density cooling header.

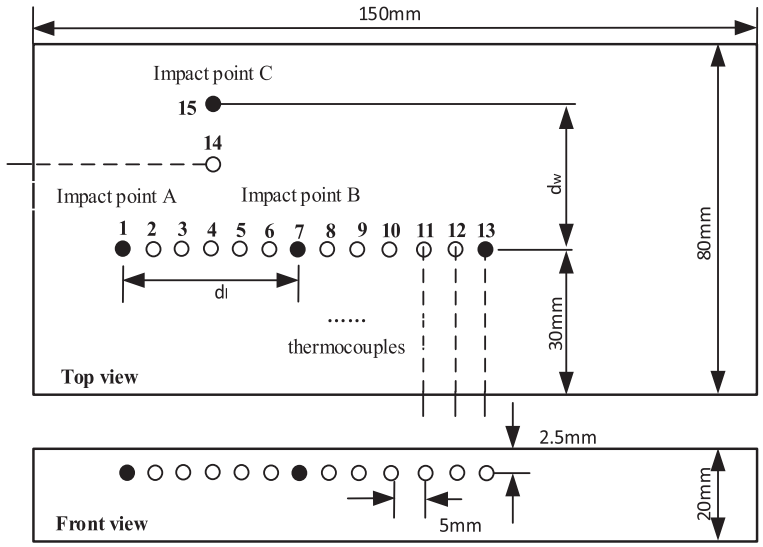

Fig. 3. Jet impingement prototype and arrangement of thermocouples.

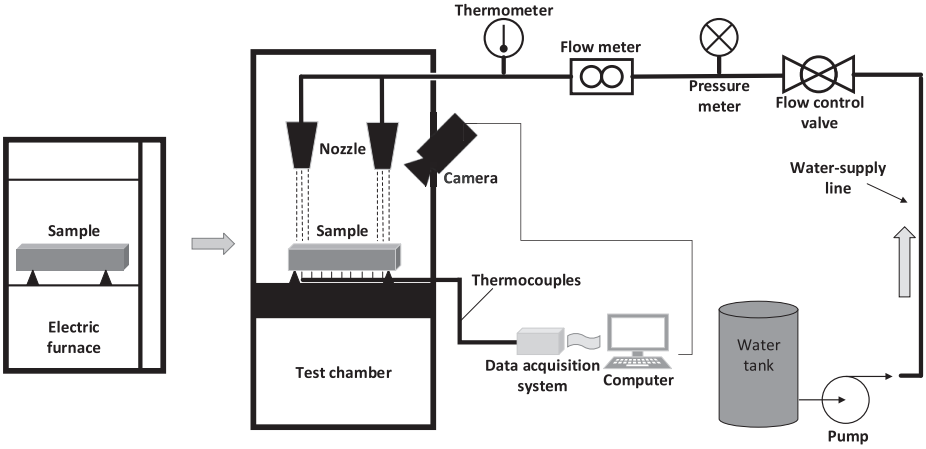

Fig. 4. Schematic of the experiment facility.

was inserted from the wide side only for the three jet test, for the interference behavior effects study of the parallel flows on the heat transfer characteristics during the three jet impingement cooling. A high-temperature glue sealed the narrow gap between the plate and the thermocouples for the measurement accuracy to be ensured. A data acquisition system with 10 channels was utilized for the data collection from the thermocouples, at an acquisition rate of 10 points per second. In order for the plate surface temperature change to be provided at an arbitrary time, an inverse heat conduction formulation, based on a sequential function specification method, was adopted for the temperature field in the thickness direction calculation.[11] The specific experimental parameters are illustrated in **Table 1**. The constant parameters include the jet length of $L = 60$ mm, the jet diameter of $D = 4$ mm and the impingement height of $H = 200$ mm. The parameter d_l was set to be the nozzle spacing length of the multi jet and the d_w was set to be the nozzle spacing width.

The experimental facility was built as presented in **Fig. 4**. The initial plate temperatures were heated slightly higher than the targeted initial cooling temperature 973 K, with consideration to the heat loss during the transfer process. Following, the plate was well positioned under the cooling water jets; the jet control valve was activated, whereas the water flowed out from a bypass pipe adjacent to the jet outlet. Once the targeted temperature was reached, the on-off valve was quickly activated and the water would impinge vertically onto the plate surface within a short time. Nev-

Table 1. Experimental variables for multi jet impingement cooling.

Test No.	Jet velocity (m/s)	Nozzle spacing d_l (mm)	Nozzle spacing d_w (mm)	Impact point A	Impact point B	Impact point C
1	3.98	–	–	1	–	–
2	3.98	20	–	1	5	–
3	3.98	30	–	1	7	–
4	3.98	40	–	1	9	–
5	1.99	40	–	1	9	–
6	2.84	40	–	1	9	–
7	6.63	40	–	1	9	–
8	2.21	30	30	1	7	15
9	3.32	30	30	1	7	15
10	6.63	30	30	1	7	15

ertheless, the initial cooling temperature fluctuation was maintained at ±10°C. During the experimental procedure, the temperatures were scanned from the thermocouples and recorded by a computer, whereas a video camera was utilized for the jets impingement cooling to be recorded. After every experiment, it is necessary to clean the surface of the plate with ethanol and dilute hydrochloric acid, because the oxide layers attached to the surface of the plate will affect HTC, just as what Wendelstorf researched, he found that the oxide layer effect on the HTC decreases with increasing stability and with decreasing thickness of the layer.[22)]

2.3. Error Analysis

The measurement errors could be divided into two components: the random errors and the systematic errors. The type K thermocouples normally display an error of approximately ±0.75%. The deviation of the thermocouple location was ±0.2 mm. The relative error of the temperature acquisition system (GRAPHTEC GL220) was approximately ±0.5%. The water temperature was controlled to 15°C within ±0.5°C. The jet velocity was controlled within a tolerance of ±0.2 m/s. The video camera frame rate in this study was 30 fps and the accuracy of the retarded wetting time herein was ±0.034 s. Also, the cumulative error in the inverse calculation of the heat flux was within ±2%.

3. Results and Discussion

3.1. Video Observation and Heat Transfer Region Analysis

The digital images are presented in **Fig. 5**, as the cooling water impinged on the plate surface, two black areas (denoted as rewetted region) appeared at the stagnant points. The rewetting occurred immediately within 0.06–0.08 s as the water jet stroke the hot surface.[23)] In the peripheral area, the plate surface was dominantly covered by the boiling film (denoted as dry region), reducing the water-solid contact possibility and inhibiting the efficient heat exchange.[16)] The wetting front region was the transition stage from the dry region to the rewetted region, with an intense boiling phenomenon. The rewetted region expanded outwards as a circle in the external area agreed well with the single impinge jet, whereas the heat transfer characteristics would be changed by the water flow interference in the central area of the double jet.

Compared to the double jet, the water flows for the three jet impingement cooling were quite violent as presented in **Fig. 6**. Once the cooling water stroke the high temperature wall, three black wetting areas formed. Afterwards, the water flows radially expanded resulting in severe turbulent flow between the impact points. From 0.33 s to 0.67 s, the wetting regions expanded outwards, whereas the water flow interference region had not yet reached the rewetted state. The fluid state tended to be stable from 1 s to 2 s, whereas the accumulated water amount at the intersection of the three fluid streams gradually increased. In the interference region, the parallel flows continuously clashed to each other, splash and returned onto the hot plate surface by gravity. The accumulated fluid on the plate surface was drained through the gap among the jets, whereas the rewetted regions were gradually connected. When the cooling time reached 4 s, the spatter height in the interference region was slightly reduced, whereas the rewetted regions continued to expand and connected as a whole.

As indicated in **Fig. 7**, the cooling water was ejected

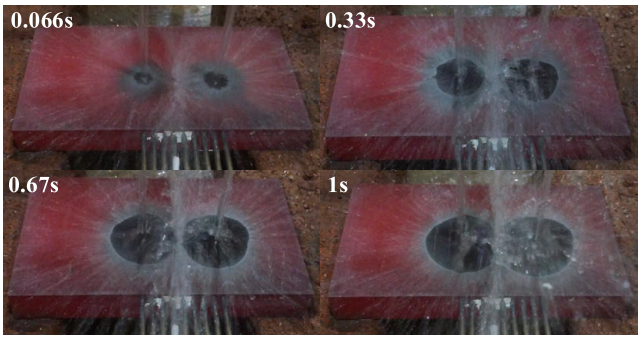

Fig. 5. Image of double jet impingement cooling.

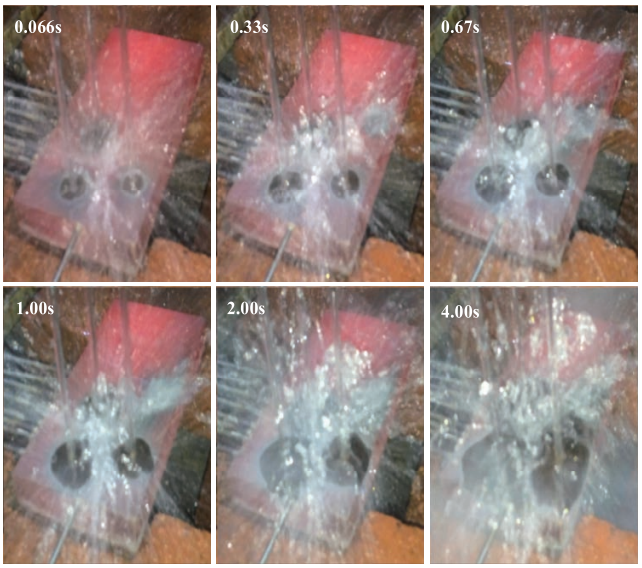

Fig. 6. Image for the three jet impingement cooling.

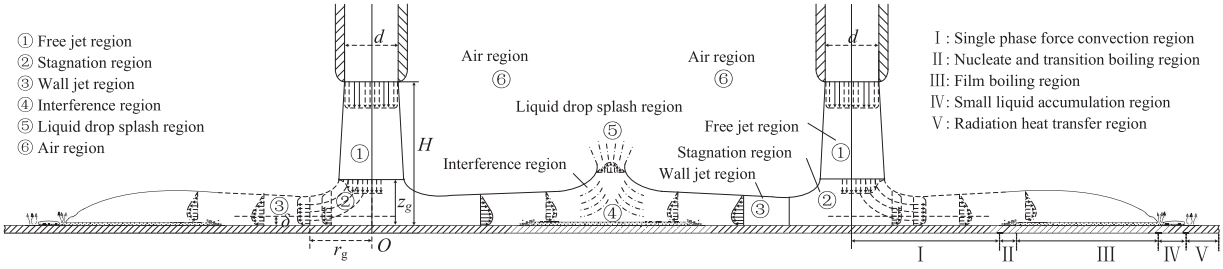

Fig. 7. Water flow and heat transfer region distribution for double jet impingement cooling.

from the nozzle in the free jet region with high vertical velocity. Following, it impinged on the plate surface and formed the stagnation region by the reaction force. The fluids consequently flowed outwards at a horizontal velocity to the wall jet region. Similarly to the single jet impingement heat transfer region distribution, the single-phase forced convection region, the nucleate boiling region, the transition boiling region, the film boiling region, the small liquid accumulation region and the radiation heat transfer region were radially distributed in the external heat transfer region. Besides, the parallel flows with a certain amount of momentum and energy collided to each other seriously and spattered upwards, creating an interference region and a liquid drop splash region between the two adjacent impact regions.

3.2. Heat Flux and Rewetting Delay Analysis for Double Jet Impingement Cooling

Although the experimental conditions in tests 1 and 2 for the single jet and the double jet impingement cooling were not the same, the instantaneous boiling curves for all measurement points evaluated by the inverse heat conduction method, behaved similar trajectories as illustrated in **Fig. 8**. The evolution of both surface temperature and heat flux against the cooling time period is plotted in **Fig. 9**.[12] The surface temperature demonstrated a slight decrease in the film boiling phase (I) and consequently exhibited a sharp decrease in both transition boiling (II) and nucleate boiling (III) phases. Finally, the surface temperature was retained to a low cooling rate in the single phase force convection phase (IV). The surface heat flux displayed a correlation trend with the surface temperature. It reached the maximum heat flux (MHF) at the conversion time periods of phase II and phase III, when the sharpest surface temperature decrease occurred being related to the wetting front expansion.

As presented in Figs. 8(a) and 8(b), the MHFs of the heat flux curves decreased as the wetting front moved outwards from the stagnant point, whereas the wetting delay time t_ds and the time to reach MHF t_{MHF}s increased, due to the parallel flow velocity u attenuation and the subcooling ΔT_{sub} increment, during the parallel water flow expansion.[12] Regarding the single jet impingement cooling, the MHF decreased from 5.25 MW/m^2 at the stagnant point to 4.29 MW/m^2 (approximately 18.3%) at r = 20 mm, whereas the t_d increased from 0.08 to 0.59 s and the t_{MHF} was prolonged from 0.8 to 1.6 s, correspondingly. In contrast, regarding the double jet with a nozzle spacing of 20 mm, the MHF difference in the internal heat transfer area was quite low with a value 5.21 MW/m^2 at the stagnant point and 4.95 MW/m^2 at r = 10 mm in the interference region. In addition, the boiling curves almost coincided in the narrow internal heat transfer region with the similar t_d and t_{MHF}.

The heat transfer characteristics in the interference region for the double jet impingement cooling under the experiments 2 to 4 are presented in **Fig. 10**, where the heat transfer capability was relatively high and the wetting delay time t_ds became shorter in contrast to the single

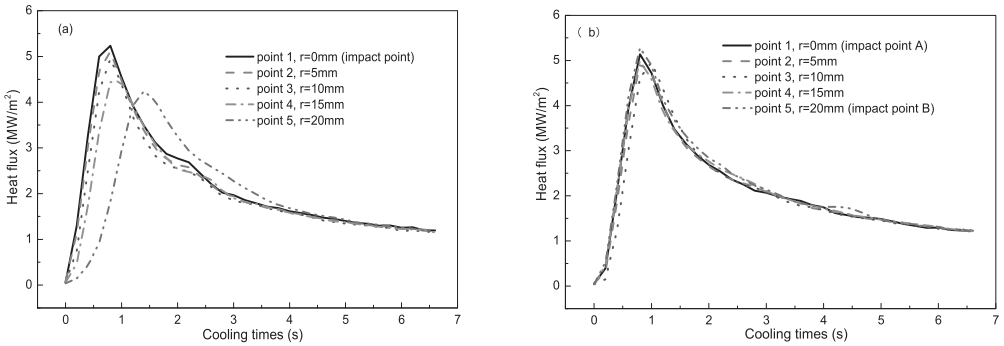

(a)Single jet impingement (b) Double jet impingement

Fig. 8. Heat flux curves for the single jet and double jet impingement cooling.

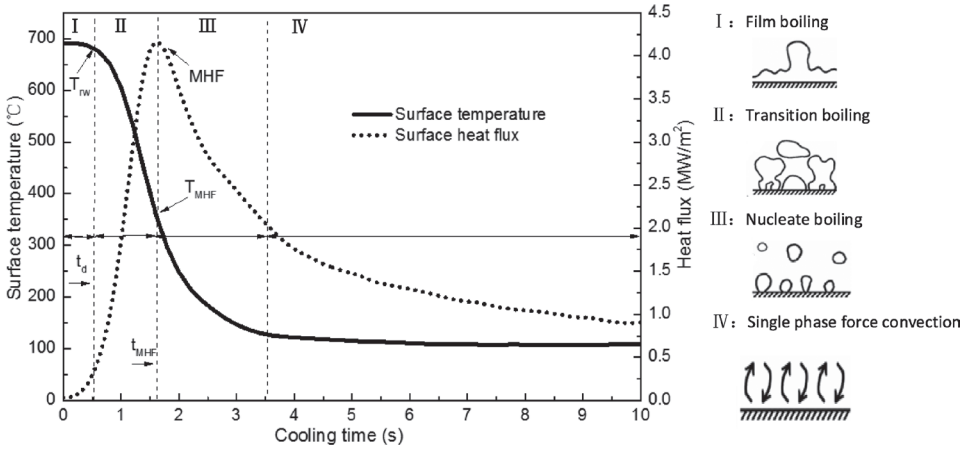

Fig. 9. Surface temperature and heat flux curve during jet impingement cooling.

jet time period in test 1. The nozzle spacing significantly affected the heat transfer capacity. The MHFs at the center of the interference region were 4.95, 4.87 and 4.73 WM/m^2 respectively for the nozzle spacing values of 20, 30 and 40 mm, whereas regarding the single jet, the MHFs were 4.94, 4.46 and 4.24 WM/m^2 at the same spatial locations r = 10, 15 and 20 mm from the impact point A, the increase ratios were 0.2%, 6.6% and 8.2% respectively. Correspondingly, the t_ds at the center of the interference region were reduced from the single jet t_ds 0.17, 0.35 and 0.59 s to 0.15, 0.19 and 0.34 s. The difference was particularly significant for the higher-sized nozzle spacing. It could be deduced, that although the parallel flow velocity was weakened, the severe interaction of the counter-parallel flows would enhance the heat transfer characteristics in the interference region for the double jet impingement cooling, if the parallel flow still retained a sufficient kinetic energy.

The MHF and t_d distributions in the internal heat transfer region at various jet velocities for experiments 5 to 7 are presented in **Figs. 11** and **12**. Apparently, the higher jet velocity contributed to the heat flux increase and accelerated the rewetting speed, especially outside the stagnation region. The MHFs were 4.96 and 5.27 MW/m^2 at the stagnant point and 4.15 and 4.86 MW/m^2 at the center of the interference region for the jet velocity values of 1.99 and 6.63 m/s. Also, at r = 20 mm in the interference region, the t_ds were 0.4, 0.6, 0.7 and 0.85 s for the jet velocities of 1.99, 2.84, 3.98 and 6.63 m/s. The shear force, which affected strongly both the growth and the detachment of the bubbles,[24] was increase along with the jet velocity, whereas the water flow velocity increment also prevented the formation of the stable film layer.[25] Karwa *et al.*[6] also reported that an increased jet velocity would enhance the bubble detachment rate from the surface and prevent the accumulation of bubbles in the rewetting front region. It was worthy to be noted that the propagation speed of the wetting front was crucial to the elevation of the cooling capacity[26] with the promotion of the water-solid interface into the nucleate boiling region with high heat transfer efficiency.

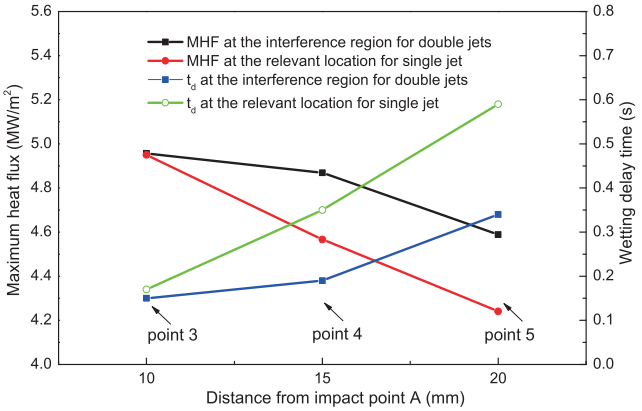

Fig. 10. MHFs and Wetting delay time tds at the interference region for double jet.

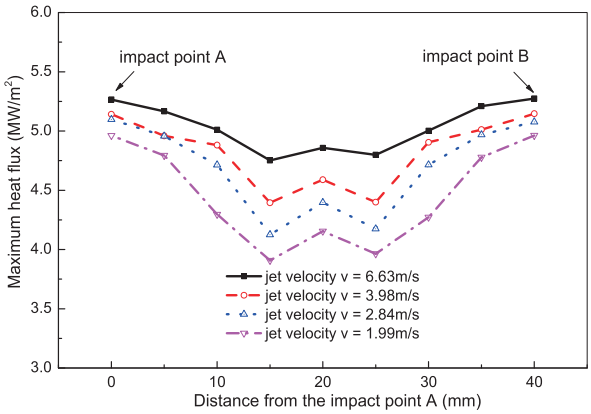

Fig. 11. MHFs for different jet velocities.

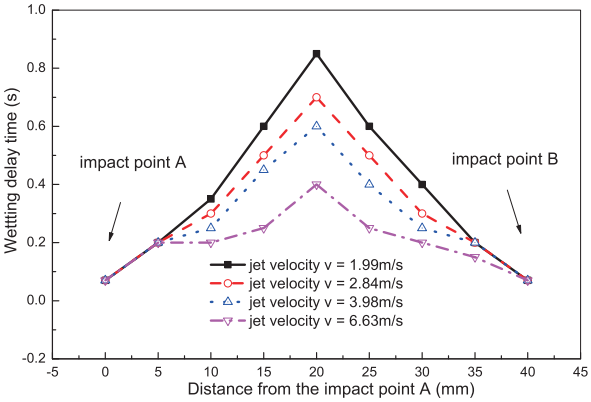

Fig. 12. Wetting delay time tds for different jet velocities.

3.3. Surface Temperature and HTC Analysis for Three Jet Impingement Cooling

The variation of surface temperature along with the cooling time period at various measurement positions for various jet velocities is illustrated in **Fig. 13**. Following the cooling water impingement on the hot plate surface for 1.0 s, the temperature around the stagnant points was displayed as the lowest temperature zone, indicating that during the free-surface multi jet impingement cooling, the heat transfer characteristic was slightly affected in the stagnation region. The temperature decreased slowly along with the spatial distance increase to the stagnant point. The temperature at the measuring point 4 in the interference region between the two adjacent jets was substantially lower than the point 10 in the parallel flow region at any given time, which proved that the heat transfer capacity in the interference region was slightly

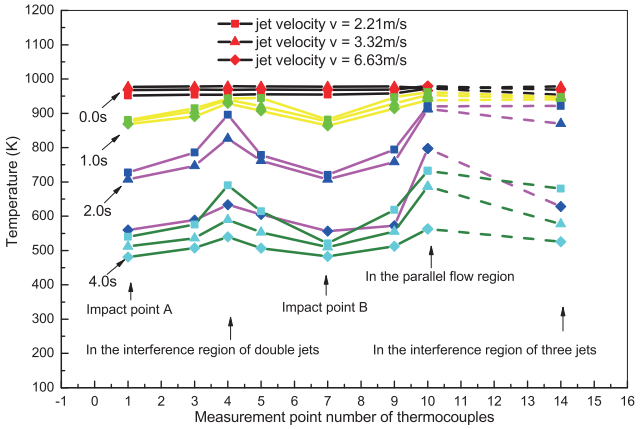

Fig. 13. Variation of surface temperature with cooling time.

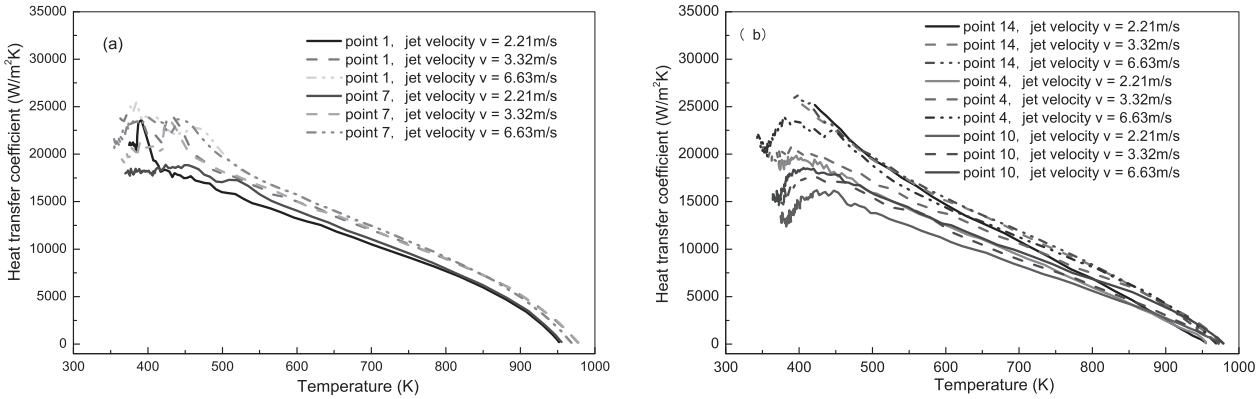

Fig. 14. HTC in different locations with the surface temperature for different jet velocities.

higher from the parallel flow region. In addition, at the measurement point 14 in the three jet cross-interference region, the surface temperature decreased slowly at first, whereas subsequently to 1 s it decreased faster. This phenomenon was ascribed to the water flow higher violent vortex, which could effectively carry away the bubbles attached onto the hot plate surface[15] and increase both the boiling frequency and the heat extraction quantity.[27]

The distributions of the heat transfer coefficient (HTC) curves were plotted for the surface temperature evolution to be further clarified. As presented in **Fig. 14**, the HTC curves for all measuring positions were nonlinear to the surface temperature for the experiments 8, 9 and 10. In general, the HTC monotonously increased whereas the surface temperature decreased from 700 to approximately 150–180°C. In contrast, the HTC curve slope gradually became flat. When the heat transfer turned into a single-phase forced convection status, the HTC curve slope began to drop sharply. Correspondingly to the heat flux, the HTC increased significantly as the jet velocity increased. Also, for different measurement positions, the HTCs significantly varied, depending to a high extent on the distribution and evolution of the water jet impinging flow and the heat transfer regions. Apparently, as presented in Fig. 14(a), the HTCs in the interference region were relatively high, second only to the stagnant point as presented in Fig. 13(b). At the jet velocity of 3.32 m/s, the HTCs at the measurement point 1 in the stagnation region, the measurement point 10 in the parallel flow region, the measurement point 4 in the interference region between the two adjacent jets and the measurement point 14 in the center of the interference region of the three jets were 15 730.87, 13 686.65 and 14 408.39, 15 171.54 W/m^2*K respectively, when the surface temperature reached 300°C. The HTC at the measurement point 4 was 5.1% higher than the value of the measurement point 10, although the latter had the same distance of 15 mm from the stagnant points. Moreover, the increment was quite significant at the measurement point 14. It could be deduced that the parallel flows interaction and agitation in both the interference and liquid drop splash regions, enhanced the heat transfer intensity.[15] The data in Fig. 14 also display that as the jet velocity increased, the HTC was further enhanced, particularly at the locations a far from the stagnant point, which resulted in the temperature distribution as presented in Fig. 13. A similar phenomenon was already mentioned by both Hauksson *et al.*[10] and Agrawal *et al.*,[8] where it was demonstrated the heat fluxes at various locations under various velocities characterized the heat transfer intensity distribution.

4. Conclusions

(1) Both the hydrodynamic structure and the heat transfer region distribution of multi jet impingement were studied experimentally. The results demonstrated that the single-phase forced convection region, the nucleate boiling region, the transition boiling region, the film boiling region, the small liquid accumulation region and the radiation heat transfer region were radially distributed within the external heat transfer region. In contrast, the parallel flows with a certain amount of momentum and energy collided to each other seriously and spattered upwards, creating an interference region and a liquid drop splash region.

(2) Similarly to the single jet case, the heat flux curves of the multi jet impingement cooling included the film boiling region, the transition boiling region, the nucleate boiling region and the single phase force convection region. The nozzle spacing increase magnified the heat transfer characteristic difference in the interference region and the jet velocity increase would increase the heat flux and accelerate the rewetting speed outside the stagnation region, which were crucial in the high density cooling header optimization in industrial applications.

(3) The variation of various measurement positions surface temperatures along with various cooling time periods was analyzed. At the same distance from the stagnant point, the surface temperature variation in the interference region was slightly faster from the parallel flow region, second only to the stagnant point. The HTC curves demonstrated that the parallel flows interaction and agitation in both the interference and the liquid drop splash regions enhanced the heat transfer intensity.

Acknowledgments

This research was supported by the National Natural Science Foundation of China (51404058) and the Fundamental Research Funds for the Central Universities (N150704005).

Nomenclature

q_s: surface heat flux (MW/m^2)
MHF: maximum heat flux (MW/m^2)

t_d: rewetting delay time (s)
t_{MHF}: cooling time when a location reach its maximum heat flux (s)
T_s: surface temperature (K)
u: jet velocity (m/s)
d: jet diameter (mm)
O: stagnation point
H: distance between the nozzle outlet to the plate surface (mm)
δ: thickness of the water flow boundary layer (mm)
r_g: distance along the wall from the stagnant point (mm)
z_g: distance from the wall in the vertical direction (mm)
r: position in the radial direction from the impact point A (mm)
d_l: length nozzle spacing (mm)
d_w: width nozzle spacing (mm)
ΔT_{sub}: liquid sub-cooling (K)
ΔT_{sup}: superheat (K)

Subscripts

l: length axis
w: width axis
s: surface of test specimen

REFERENCES

1) S. Tang, Z. Y. Liu, G. D. Wang and R. D. K. Misra: *Mater. Sci. Eng. A*, **580** (2013), 257.
2) S. V. Ravikumar, J. M. Jha, S. S. Mohapatra, S. K. Pal and S. Chakraborty: *J. Iron Steel Res. Int.*, **84** (2013), 1157.
3) B. Wang, Z. Wang and G. Wang: Iron and Steel Technology Conf., and Exposition (AISTech 2014), AIST, Warrendale, PA, (2014), 3073.
4) W. Timm, K. Weinzierl and A. Leipertz: *Int. J. Heat Mass Transf.*, **46** (2003), 1385.
5) H. Robidou, H. Auracher, P. Gardin and L. Michel: *Exp. Therm. Fluid Sci.*, **26** (2002), 123.
6) N. Karwa, T. Gambaryan-Roisman, P. Stephan and C. Tropea: *Exp. Therm. Fluid Sci.*, **35** (2011), 1435.
7) J. Hammad, Y. Mitsutake and M. Monde: *Int. J. Therm. Sci.*, **43** (2004), 743.
8) C. Agrawal, R. Kumar, A. Gupta and B. Chatterjee: *Int. J. Therm. Sci.*, **71** (2013), 310.
9) S. V. Ravikumar, J. M. Jha, S. S. Mohapatra, A. Sinha, S. K. Pal and S. Chakraborty: *Heat Mass Transf.*, **49** (2013), 1509.
10) A. T. Hauksson, D. Fraser, V. Prodanovic and I. Samarasekera: *Ironmaking Steelmaking*, **31** (2004), 51.
11) B. Wang, X. Guo, Q. Xie, Z. D. Wang and G. D. Wang: *Int. J. Heat Mass Transf.*, **101** (2016), 844.
12) B. Wang, D. Lin, Q. Xie, Z. D. Wang and G. D. Wang: *Appl. Therm. Eng.*, **100** (2016), 902.
13) M. J. Kwon and I. S. Park: *ISIJ Int.*, **53** (2013), 1042.
14) I. S. Park: *ISIJ Int.*, **51** (2011), 743.
15) Q. Xie, B. Wang, Y. Wang, Z. D. Wang and G. D. Wang: *ISIJ Int.*, **56** (2016), 1210.
16) A. K. Nallathambi and E. Specht: *J. Mater. Process. Technol.*, **209** (2009), 5325.
17) T. L. Fu, Z. D. Wang, Y. Li, J. D. Li and G. D. Wang: *Appl. Therm. Eng.*, **70** (2014), 800.
18) L. F. G. Greers, K. Hanjalic and M. J. Tummers: *J. Fluid Mech.*, **546** (2005), 255.
19) D. M. Kercher and W. Tabakoff: *J. Eng. Gas Turbines Power*, **92** (1970), 73.
20) D. E. Metzger, L. W. Florschuetz, D. I. Takeuchi, R. D. Behee and R. A. Berry: *J. Heat Transf.*, **101** (1978), 526.
21) H. Wang, W. Yu and Q. Cai: *J. Mater. Process. Technol.*, **212** (2012), 1825.
22) R. Wendelstorf, K. H. Spitzer and J. Wendelstorf: *Int. J. Heat Mass Transf.*, **51** (2008), 4892.
23) C. Agrawal, R. Kumar, A. Gupta and B. Chatterjee: *Exp. Therm. Fluid Sci.*, **42** (2012), 25.
24) J. F. Klausner, R. Mei, D. M. Bernhard and L. Z. Zeng: *Int. J. Heat Mass Transf.*, **36** (1993), 651.
25) M. A. Wells, D. Li and S. L. Cockcroft: *Metall. Mater. Trans. B*, **32** (2001), 929.
26) K. H. M. Abdalrahman, U. Alam and E. Specht: 14th Int. Heat Transfer Conf., ASME, New York, (2010), 475.
27) A. K. Mozumder, M. Monde and P. L. Woodfield: *Int. J. Heat Mass Transf.*, **48** (2005), 5395.